Post liver transplantation acute kidney injury in a rat model of syngeneic orthotopic liver transplantation

Jun Wang[1,3], Zhiyong Du[2,3], Wen Zhang[1], Baosan Han[2], Chenghong Peng[2] and Nan Chen[1]

Acute kidney injury (AKI) is a frequent complication after liver transplantation (LT). The mechanism of post-LT AKI remains unclear. We used the rat model of syngeneic orthotopic LT (SOLT) to investigate the mechanism of post-LT AKI. We hypothesized that the condition of the graft, rather than intraoperative hemodynamic instability, has an important role in post-LT AKI in the SOLT model. Rats were randomly assigned into four groups: sham-operated group; vessel-clamped group; full-size LT group; and reduced-size LT group. We identified AKI in both full-size and reduced-size LT groups. In addition to renal tubular necrosis and apoptosis, renal peritubular capillary injury was also present. Pathological changes were more severe in the reduced-size than in the full-size LT group. We found that the systemic inflammatory response induced by LT was the initiating factor in post-LT AKI. This is the first study to investigate the pathological mechanism of AKI in an animal model of SOLT. Our results demonstrate that protection of the liver graft and inhibition of the systemic inflammatory response are vital in reducing the risk of post-LT AKI.
Laboratory Investigation (2011) 91, 1158–1169; doi:10.1038/labinvest.2011.59; published online 23 May 2011

Orthotopic liver transplantation (OLT) is indicated for patients with end-stage liver disease of almost any etiology. Acute kidney injury (AKI) is a frequent complication after OLT and unfavorably affects prognosis post-LT (LT). AKI occurs in ∼80% of cases in the first 48 h after LT.[1] Post-LT AKI increases length of stay, cost, and mortality,[2] and is an important risk factor for chronic kidney disease (CKD) and end-stage renal disease (ESRD).[3] Cohen et al[4] reported an incidence of CKD (GFR <40 ml/min) of 27.5% post-LT at 5-year follow-up. Gonwa et al[5] quoted the incidence of ESRD to be 9.5% 13 years post-LT.

Although AKI post-LT is common, its mechanism remains unclear. Risk factors such as intraoperative hemodynamic instability, post-reperfusion graft function, infection, and nephrotoxic drugs may predispose to post-LT AKI.[6] Because the use of renal biopsy is limited in this scenario, it is difficult to elucidate the mechanism of post-LT AKI by clinical studies. Therefore, experimental research using animal models is required.

We used a syngeneic orthotopic LT (SOLT) rat model to investigate the mechanism of post-LT AKI. We used the

different sized LT models to study the relationship between graft function and renal injury. A vessel-clamped group, mimicking intraoperative hemodynamic instability, and a model for systemic inflammatory response syndrome were studied in their relationship to post-LT AKI.

MATERIALS AND METHODS
Murine Model of SOLT

Animals were treated according to the Guidelines for the Care and Use of Laboratory Animals of Shanghai Jiao Tong University and maintained in a laminar flow, pathogen-free atmosphere. SOLT was performed using adult male Sprague–Dawley rats (250–280 g, SLAC, Shanghai, China) as donors and recipients. The operation was performed according to the Kamada and Calne's cuff technique.[7] Rats were randomized into four groups with 40 rats in each group as follows: (a) sham-operated group (sham); (b) full-size orthotopic LT group (100% SOLT); (c) reduced-size orthotopic LT group (50% SOLT); and (d) vessel-clamped group (VC). Sham-operated rats underwent laparotomy and identical liver manipulations without the vascular occlusion. Full-size

[1]Department of Nephrology, Ruijin Hospital, School of Medicine, Shanghai Jiao Tong University, Shanghai, PR China and [2]Department of Surgery, Ruijin Hospital, School of Medicine, Shanghai Jiao Tong University, Shanghai, PR China
Correspondence: Dr N Chen, MD, Department of Nephrology, Ruijin Hospital, School of Medicine, Shanghai Jiao Tong University, Shanghai 200025, PR China and CH Peng, MD FACS, Department of Surgery, Ruijin Hospital, School of Medicine, Shanghai Jiao Tong University, Shanghai 200025, PR China.
E-mails: chen-nan@medmail.com.cn and chhpeng@188.com
[3]These authors contributed equally to this work.

and reduced-size SOLT were performed as described previously.[7,8] The liver was perfused with 15 ml of lactated Ringer's solution at 4°C through the abdominal aorta and the excised graft was stored in lactate Ringer's solution at 4°C. Cold ischemic time was 55–60 min. The anhepatic phase of both full-size and half-size orthotopic LTs was 15–20 min. In the VC group, rats underwent laparotomy and the infra-hepatic inferior vena cava (IHIVC) was clamped. The IHIVC was also clamped before dissection in SOLT rats. The duration of the unstable renal hemodynamic state was 25 min. Animals were killed at either 6, 24, or 72 h after surgery. Liver and left kidney tissue was collected, as well as plasma for measurement of alanine aminotransferase (ALT), creatinine (Cr), and inflammatory cytokines.

Assessment of Liver and Kidney Dysfunction

Blood samples were centrifuged at 3000 g for 10 min at 4°C, and plasma ALT and Cr were assessed by an auto-analyzer (Beckman DXC600).

Histology and Quantification of Hepatic and Renal Injury

The liver and kidney sections were stained with hematoxylin–eosin and periodic-acid Schiff. Samples were analyzed for tubular cell necrosis, tubular dilation, intratubular detachment ($\times 200$), and evaluated in a blinded manner by a nephrologist. Abnormalities were graded by a semi-quantitative score (0 to 4+): 0, no abnormalities; 1+, changes affecting <25% of the tubules; 2+, 25% to 50%; 3+, 50% to 75%; 4+, >75%.

Immunohistochemistry and Immunofluorescence Microscopy

Immunohistochemical analysis was carried out on paraffin-embedded sections. Sections were incubated with mouse anti-CD68 monoclonal antibody (1:200, Serotec, Oxford, UK)

for 12 h to 18 h at 4°C. To evaluate staining, a peroxidase kit (Zymed, South San Francisco, CA, USA) was used. For immunofluorescence microscopy, kidneys were perfusion fixed with 2% paraformaldehyde and sectioned at 5 μm. Sections were incubated with a mouse monoclonal anti-rat endothelial cell antibody (RECA; 1:50, Abcam, Cambridge, UK) for 12 to 18 h at 4°C. Then immunofluorescence was performed using an Alexa-488 conjugated secondary antibody (Invitrogen, Carlsbad, CA, USA). The negative control was carried out with the isotype control antibody.

Detection of Renal Apoptosis with *In Situ* Terminal Deoxynucleotidyl Transferase-Mediated dUTP Nick End-Labeling (TUNEL)

The TUNEL assay using an *In Situ* Cell Death Detection Kit (Calbiochem, Cambridge, MA, USA) was used. For detection of tubular cell apoptosis, the TUNEL assay was followed by Rhodamine-labeled Lectin Lens Culinaris Agglutinin (Vector Laboratories, Burlingame, CA, USA). Slides were viewed by confocal microscopy (Zeiss LSM510). For detection of peritubular capillary (PTC) endothelial apoptosis, the TUNEL assay was followed by incubation with RECA (1:50) for 12 h at 4°C. In all, 10 random fields were counted for every kidney at $\times 400$ magnification. Apoptotic nuclei-positive cells per field were counted and the results expressed as TUNEL-positive cells/high power field.

Calculation of Peritubular Microvasculature Density

To calculate peritubular microvasculature density by RECA staining, 10 random fields were counted for every renal section at $\times 400$ magnification using a Leica DX1000 fluorescence microscope. Quantification of endothelial volume density using overlapping orthogonal grids was as described previously.[9]

Table 1 List of primers used in this study

Gene	Forward primer	Reverse primer
IL-6	5′-GATTGTATGAACAGCGATGATG-3′	5′-CTCCAGGTAGAAACGGAACTC-3′
IL-1β	5′-AAGATGGAAAAGCGGTTTG-3′	5′-GGGAAGGCATTAGGAATAGTG-3′
TNF-α	5′-CCCAATCTGTGTCCTTCTAACT-3′	5′-CACTACTTCAGCGTCTCGTGT3′
MCP-1	5′-GCTGGAGAACTACAAGAGAATC-3′	5′TAGGGTGATGCAATTTTATAG-3′
MMP-9	5′-CCCAGATGATGGGAGAGAAG-3′	5′-TATGATGGTGCCACTTGAGG-3′
VEGF-α	5′-TGGTCTTTCGTCCTTCTTAGAG-3′	5′-GATGGGTTTGTCGTGTTTC-3′
TSP-1	5′-AGTCCAGCAGCCGCTTCTAC-3′	5′-CTTTCCAGCCAATGTGACGAG-3′
GAPDH	5′-CAAGGTCATCCATGACAACTTTG-3′	5′-GTCCACCACCCTGTTGCTGTAG-3′

Abbreviations: *GAPDH*, glyceraldehydes-3-phosphate dehydrogenase; *IL-1β*, interleukin-1β; *IL-6*, interleukin; *MCP-1*, monocyte chemotactic protein-1; *MMP-9*, metalloproteinase 9; *TNF-α*, tumor necrosis factor-α; *TSP-1*, thrombospondin-1.

RNA Isolation and Quantitative Real-Time PCR (qRT-PCR)

Total RNA was isolated from frozen renal tissue and liver tissue using TRIzol reagent (Invitrogen). Total RNA was reverse transcribed using the First Strand cDNA Synthase kit (Fermentas, Vilnius, Lithuania) to generate first-strand cDNA.

qRT-PCR was carried out using Bio-rad Opticon2 (Bio-rad, Hercules, CA, USA) using the SYBRgreen RT-PCR master mix reagents kit (Toyobo, Osaka, Japan). The sequences of the specific primer pairs for VEGF, matrix metalloproteinase 9 (MMP-9), interleukin-6 (IL-6), tumor necrosis factor-α (TNF-α), IL-1β, thrombospondin-1 (TSP-1), monocyte chemotactic protein-1 (MCP-1), and glyceraldehydes-3-phosphate dehydrogenase are shown in Table 1. For data analysis, the $2^{-\Delta\Delta Ct}$ method was used with a Microsoft Excel spreadsheet containing algorithms provided by the manufacturer.

Protein Isolation and Western Blotting

Kidney samples (100 mg) were solubilized in ProteoJET Mammalian Cell Lysis Reagent (Fermentas) according to the manufacturer's instructions. The protein concentration of the supernatants was determined by a BCA assay (Pierce, Rockford, IL, USA). Proteins were fractionated in SDS-polyacrylamide gels and western blot according to standard protocols. β-Actin (Santa Cruz Biotechnology, Santa Cruz, CA, USA) was used as a measure for protein loading. Chemiluminescent signals were visualized using FujiFilm LAS1000 image acquisition system.

Enzyme-Linked Immunosorbent Assay

Plasma TNF-α and IL-6 levels were measured by the rat TNF-α and IL-6 ELISA kit according to the manufacturer's instructions (Rapidbio, West Hills, CA, USA).

Statistical Analyses

The data were expressed as mean ± s.e.m. and were analyzed with one-way analysis of variance plus Tukey's *post hoc* multiple comparison test for multiple comparison. Non-parametric data was analyzed by the Kruskal–Wallis test. A P-value of <0.05 was considered statistically significant.

RESULTS

Hepatic and Renal Dysfunction after LT

To determine survival, rats were assessed for a total of 14 days in a preliminary experiment. The survival rate of sham, VC, 100% SOLT, and 50% SOLT rats was 100% ($n=5$), 90% ($n=10$), 80% ($n=10$), and 70% ($n=10$), respectively (Figure 1).
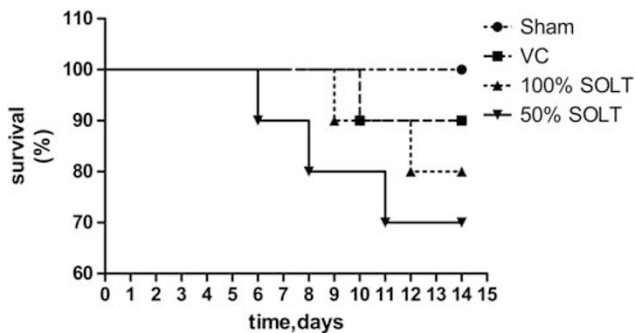

Figure 1 Postoperative survival in each group. Overall animal survival was compared in each group until 14 days postoperatively. On postoperative day 5, all animals were alive. On postoperative day 14, the survival rate of VC, 100% SOLT, and 50% SOLT rats was 90, 80, and 70%. No significant difference in survival was found between groups. ($n=5$ sham, $n=10$ VC, 100% SOLT, and 50% SOLT).
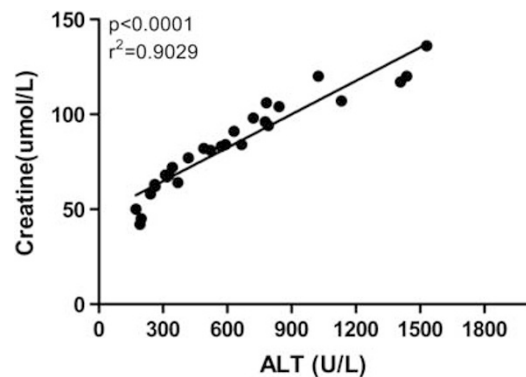

Figure 3 Correlation between plasma ALT and Cr values. $P<0.0001$ and $r^2=0.9029$. Rats were killed at 6, 24, and 72 h after LT ($n=28$).
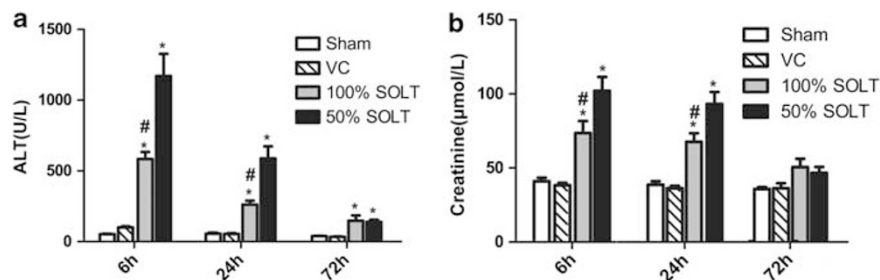

Figure 2 Postoperative serum ALT and Cr in each group. Serum ALT and Cr were determined at 6, 24, and 72 h postoperatively. *$P<0.05$ *versus* sham group, #$P<0.05$ *versus* 50% SOLT group. Data are expressed as the mean ± s.e.m. ($n=6$ at 6 h, 8 at 24 h, and 6 at 72 h).

Plasma ALT and Cr levels were normal after surgery in both sham and VC groups. In all, 100% SOLT rats developed hepatic dysfunction with significant rise of ALT at 6 and 24 h after LT. In all, 100% SOLT rats also developed renal dysfunction with an obvious rise in Cr at 6 and 24 h after LT. There was more severe hepatic and renal dysfunction in 50% of SOLT rats at 6 and 24 h after LT (Figure 2). A positive correlation between the severity of hepatic (ALT) and renal (Cr) dysfunction was observed ($P < 0.0001$, $r^2 = 0.9029$; Figure 3). LT therefore has a negative effect on both hepatic and renal function; renal dysfunction is positively related to hepatic dysfunction.

LT Results in Morphological Changes in the Liver and Kidney

By light microscopy, we observed vacuolar changes in the cytoplasm of hepatocytes and sinusoidal congestion in the liver of SOLT rats (Figure 4). In the renal sections, we demonstrated multifocal acute tubular injury as evidenced by loss of brush border, flattening and loss of tubular epithe-lium, hyaline casts, medullary congestion, and hemorrhage. The tubular injury in 50% SOLT rats was more severe than in 100% SOLT rats. The renal morphology of VC and sham rats was near normal (Figure 5).

Increased Apoptosis of Renal Tubular cells at 24 h after LT

To detect apoptosis of renal tubular cells, we double stained the renal tubular epithelium with TUNEL and Lens culinary lectin (epithelial cell label). A significant increase in the number of TUNEL-positive cells was detected in renal sections of 100% SOLT rats with respect to VC and sham rats. A TUNEL-positive signal was more marked in 50% SOLT rats compared with 100% SOLT rats (Figure 6a–e). To confirm and quantify apoptosis in the renal tissue, active caspase-3 tissue protein expression was measured by western blot. The expression of cleaved caspase-3 in renal tissue was more demonstrable in SOLT rats (Figure 6f–g). Thus, liver dysfunction induces increased apoptosis of renal tubular epithelium.
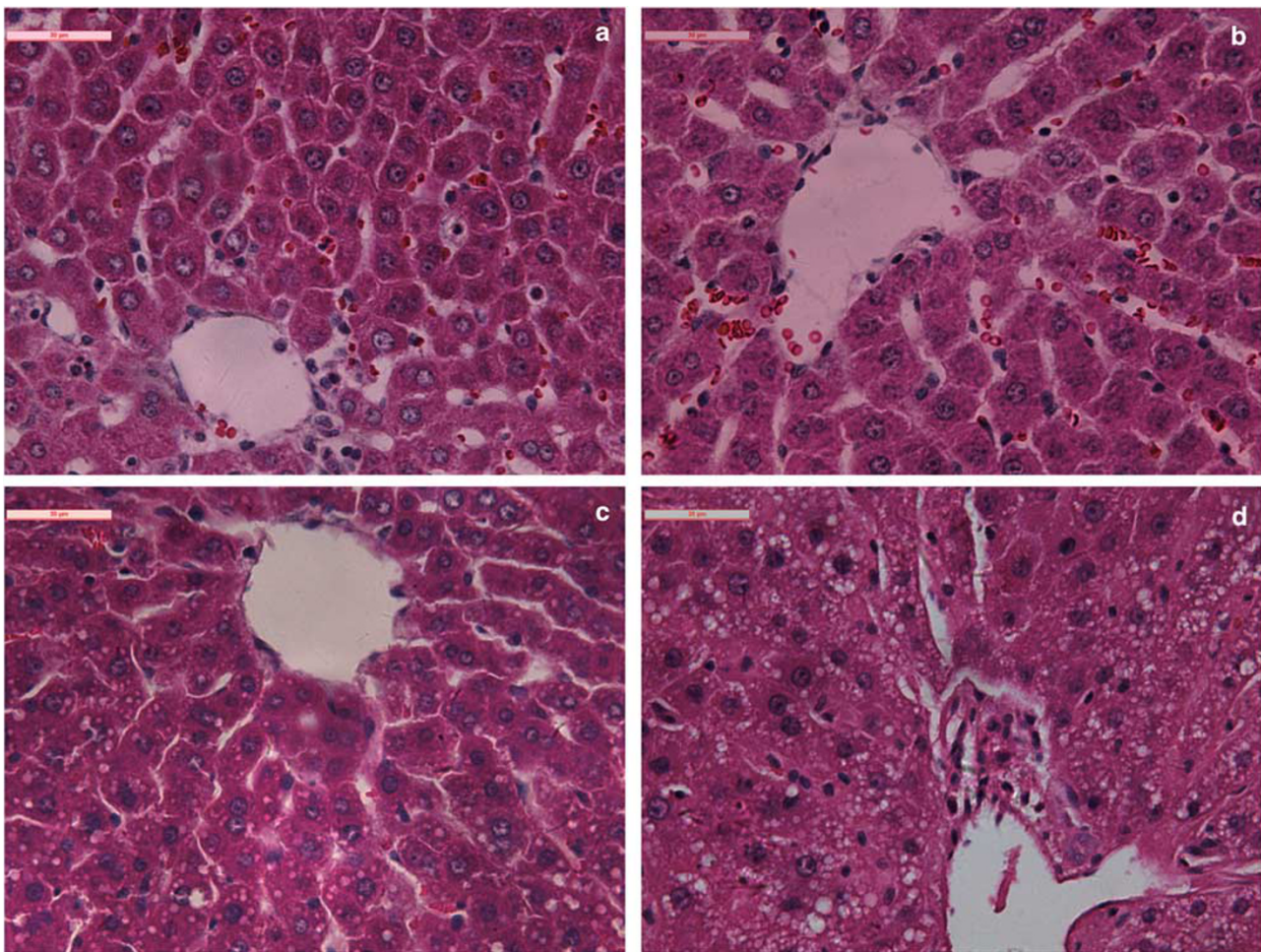

Figure 4 Histological evaluation of liver grafts at 24 h postoperatively. (**a**) Sham-operated group; (**b**) vessel-clamped group; (**c**) 100% SOLT group; (**d**) 50% SOLT group. Scale bars: 30 μm.
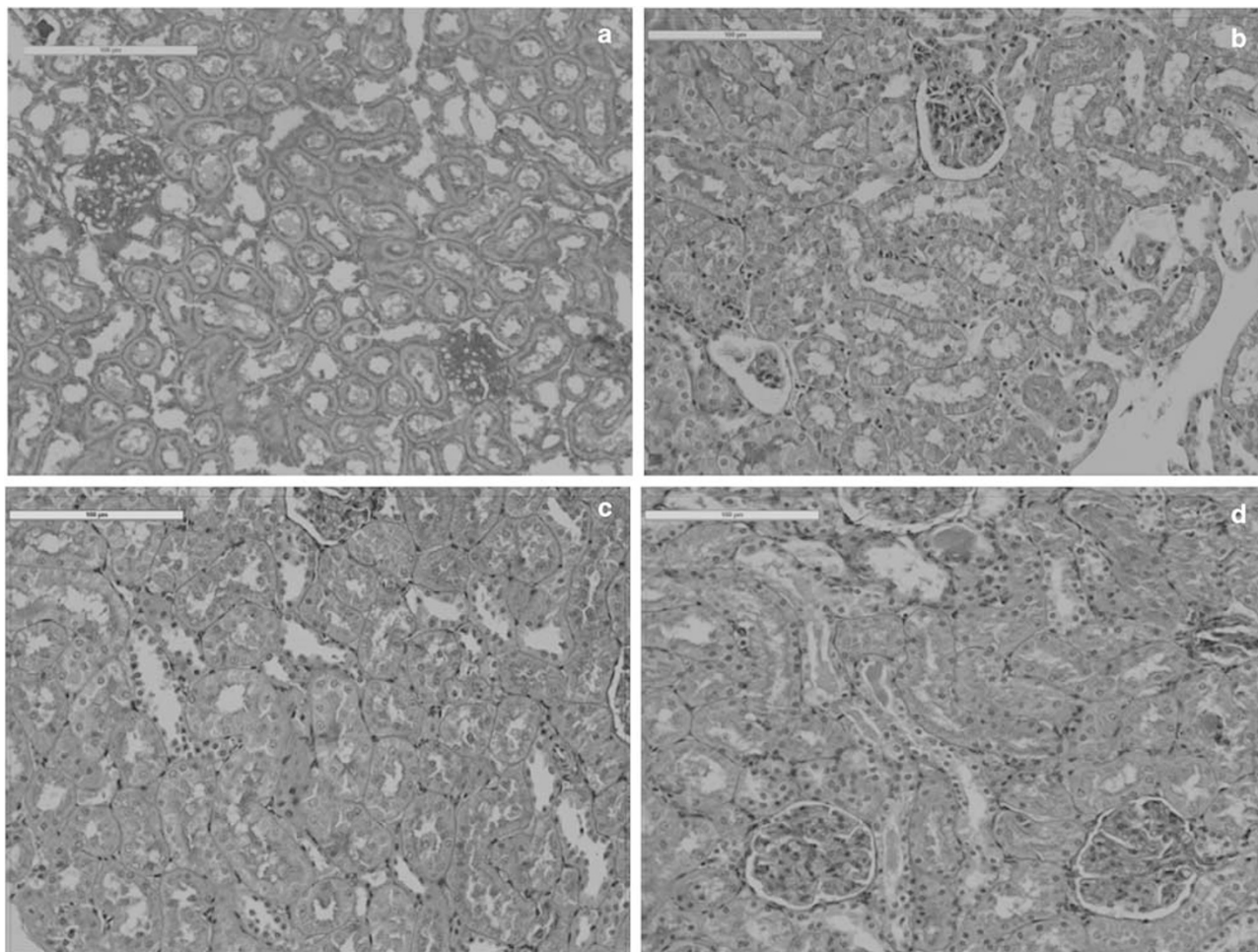
Figure 5 Histological evaluation of renal tissue obtained 24 h postoperatively. (**a–d**) Periodic acid-Schiff staining; (**a**) sham-operated group; (**b**) vessel-clamped group; (**c**) 100% SOLT group; (**d**) 50% SOLT group. (**e**) Semiquantitative scoring of histological injury ($n = 8$). Data are expressed as the mean ± s.e.m. *$P < 0.05$ *versus* sham and VC; #$P < 0.05$ *versus* 50% SOLT. Scale bars: 100 μm.

Rarefaction of Renal PTC and Increased Apoptosis of PTC Endothelium after LT

To investigate PTC endothelium injury, we used immuno-fluorescence to evaluate PTC integrity and PTC endothelium apoptosis. By morphometric analysis of RECA-labeled PTC endothelium, we found a marked reduction in volume density of PTC endothelium in SOLT rats compared with VC and sham rats. The volume density of PTC endothelium in 50%

SOLT rats was less compared with 100% SOLT rats (Figure 7a–e). By double staining the PTC endothelium with RECA and TUNEL, we found an increased density of TUNEL-positive endothelium in SOLT rats with respect to VC and sham rats. TUNEL-positive endothelium was more demonstrable in 50% SOLT rats compared with 100% SOLT rats (Figure 7f–j). Thus, LT causes injury of the renal PTC endothelium.

Upregulated Expression of Inflammatory Cytokines in Liver Tissue

We determined the level of inflammation in liver tissue by measuring the mRNA of inflammatory cytokines (IL-6, IL-1β, TNF-α, and MCP-1). There was a significant increase of IL-6, IL-1β, TNF-α, and MCP-1 mRNA levels in the liver of SOLT rats at 6 h after surgery. mRNA was higher in 50%
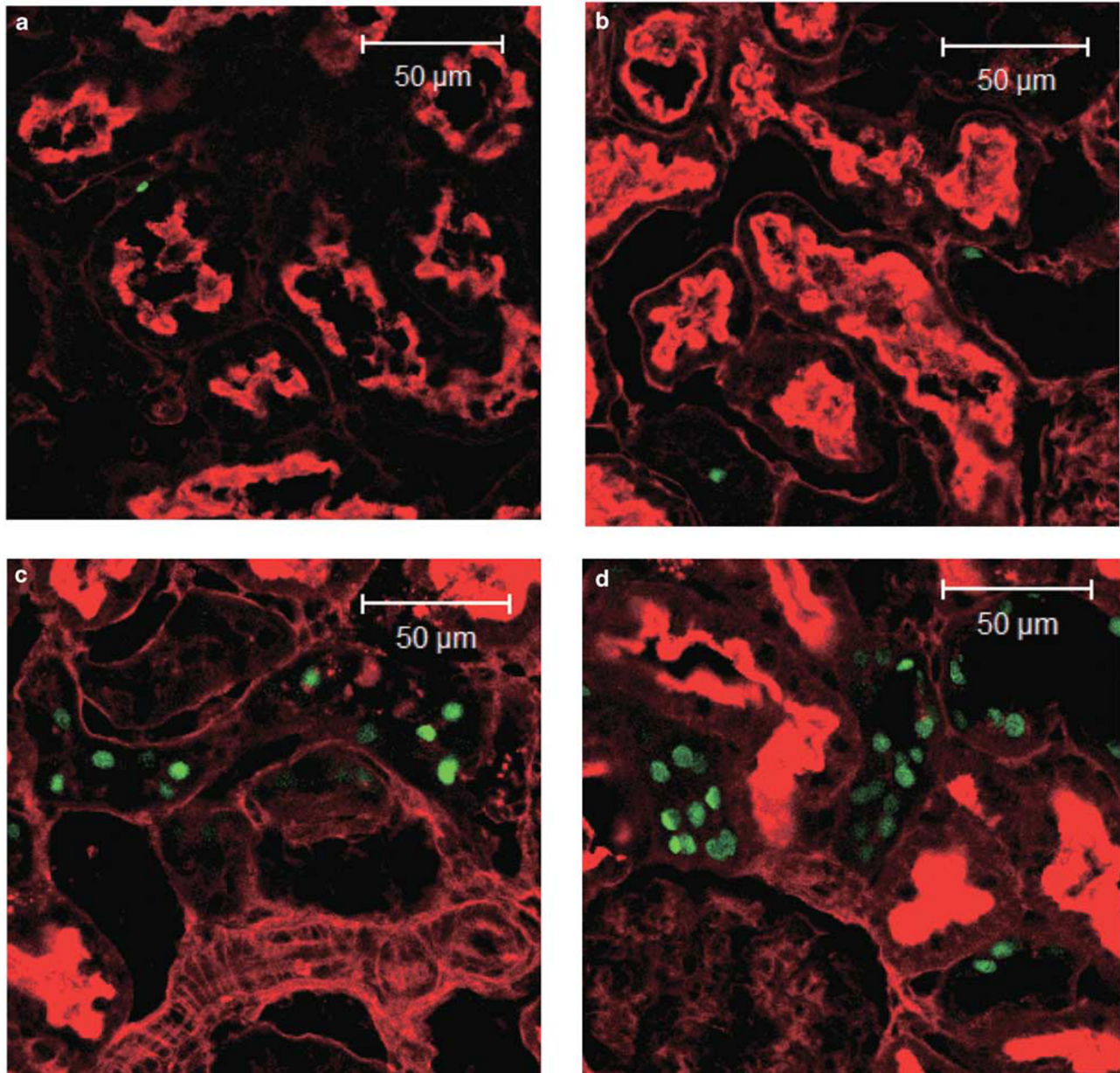

Figure 6 Detection of apoptosis in the kidney at 24 h postoperatively. (a–d): Representative fluorescence photomicrographs of renal tissue obtained at 24 h postoperatively. Selected areas were digitally enlarged to show apoptosis of renal tubular epithelium. Co-staining with TUNEL (green) and rhodamine-labeled LCA (red) identified tubular epithelial apoptosis. (a) Sham-operated group; (b) vessel-clamped group; (c) 100% SOLT group; (d) 50% SOLT group. (e) The number of TUNEL-positive cells was quantified on 10 images/slide and expressed as cells per high power field ($n = 8$). Data are expressed as the mean ± s.e.m. *$P < 0.05$ *versus* sham and VC; #$P < 0.05$ *versus* 50% SOLT. Scale bars: 100 μm. (f) Representative immunoblotting of active caspase-3 protein expression in kidney tissue homogenates obtained at 24 h after surgery. (g) Densitometric quantification of active caspase-3. Data are expressed as the mean ± s.e.m. *$P < 0.05$ *versus* sham and VC; #$P < 0.05$ *versus* 50% SOLT.
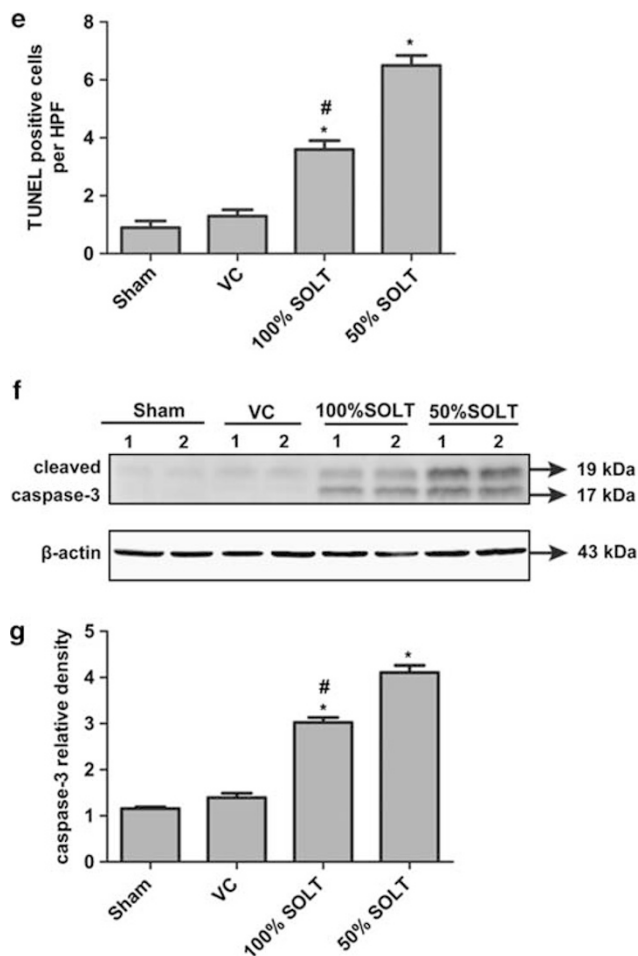
Figure 6 Continued.

SOLT rats than in 100% SOLT rats (Figure 8). Thus, the inflammatory response in the liver graft is induced after LT.

Increased Expression of Serum TNF-α and IL-6 after LT

We detected the expression of TNF-α and IL-6 in the serum by ELISA. The concentration of TNF-α and IL-6 was upregulated significantly in SOLT rats at 6 h after surgery. More obvious upregulation of TNF-α and IL-6 was observed in 50% SOLT rats when compared with 100% SOLT rats (Figure 9). Thus, LT causes the increased level of pro-inflammatory cytokines in circulation.

Increased Macrophage Infiltration and Upregulated Expression of Inflammatory Cytokines in Renal Tissue after LT

We determined the level of macrophage infiltration in the renal tissue by analysis of the macrophage labeled with CD68/ED-1. Macrophage infiltration was not detected in the renal sections of sham or VC rats. LT resulted in the recruitment of macrophages into renal tissue, especially in 50% SOLT rats (Figure 10). Macrophage infiltration in the renal tissue is

considered one of the major sources of IL-6, IL-1β, and TNF-α. In contrast to sham and VC rats, there was a significant increase of IL-6, IL-1β, and TNF-α mRNA in SOLT rat kidneys at 6 and 24 h after surgery. No significant changes of IL-6, IL-1β, and TNF-α mRNA expression were observed 72 h after surgery. A significant increase of IL-6, IL-1β, and TNF-α mRNA expression existed in 50% SOLT rats as compared with 100% SOLT rats. The different IL-6, IL-1β, and TNF-α protein levels at 24 h agreed with the increases observed in their respective mRNA levels at the same time points (Figure 11). Thus, the inflammatory response in renal tissue is induced after LT.

Renal VEGF Expression Decreases after LT

At 6 and 24 h after surgery, LT resulted in decreased VEGF mRNA expression in SOLT rats when compared with sham and VC rats. Protein expression was also decreased in SOLT rats at 24 h after surgery. This was more marked in 50% SOLT rats compared with 100% SOLT rats (Figure 12a, d, g). Therefore, renal VEGF expression is suppressed by LT.

Renal MMP-9 and TSP-1 Expression Increases after Live Transplantation

At 6 and 24 h after surgery, MMP-9 and TSP-1 mRNA expression was increased in SOLT rats with respect to sham and VC rats. The respective proteins were also increased in SOLT rats 24 h after surgery. There was a more obvious increase of MMP-9 and TSP-1 mRNA expression in 50% compared with 100% SOLT rats (Figure 12b, c, e, f, h, i). Therefore, renal MMP-9 and TSP-1 expression is enhanced by LT.

DISCUSSION

In our SOLT rat model, typical characteristics of post-LT AKI including renal tubule injury, PTC rarefaction, and inflammatory reaction were seen. The renal injury was instigated by the circulating pro-inflammatory factors released from the liver graft. The severity of AKI was relative to graft dysfunction.

Renal injury post-LT included tubular injury and PTC rarefaction. We found typical signs of acute renal tubule injury, including tubule apoptosis, tubule cast formation, and proximal tubule simplification. We also showed marked renal PTC injury including decreased PTC density and increased PTC endothelium apoptosis. PTC rarefaction has also been proved in human kidney transplants and murine models of renal ischemia reperfusion injury (IRI).[10,11] In a mouse model of AKI induced by liver IRI, Lee et al[12] demonstrated marked PTC endothelium apoptosis 24 h after reperfusion. Apoptosis of endothelial cells results in detachment of endothelium from the matrix, increasing thrombin formation.[13] This subsequently induces PTC flow cessation. The loss of renal microcirculation impairs oxygen delivery to renal tubular cells; the resultant hypoxia promotes the progression of renal tubule injury.[14] Clarification of the mechanism of PTC rarefaction post-LT is necessary.
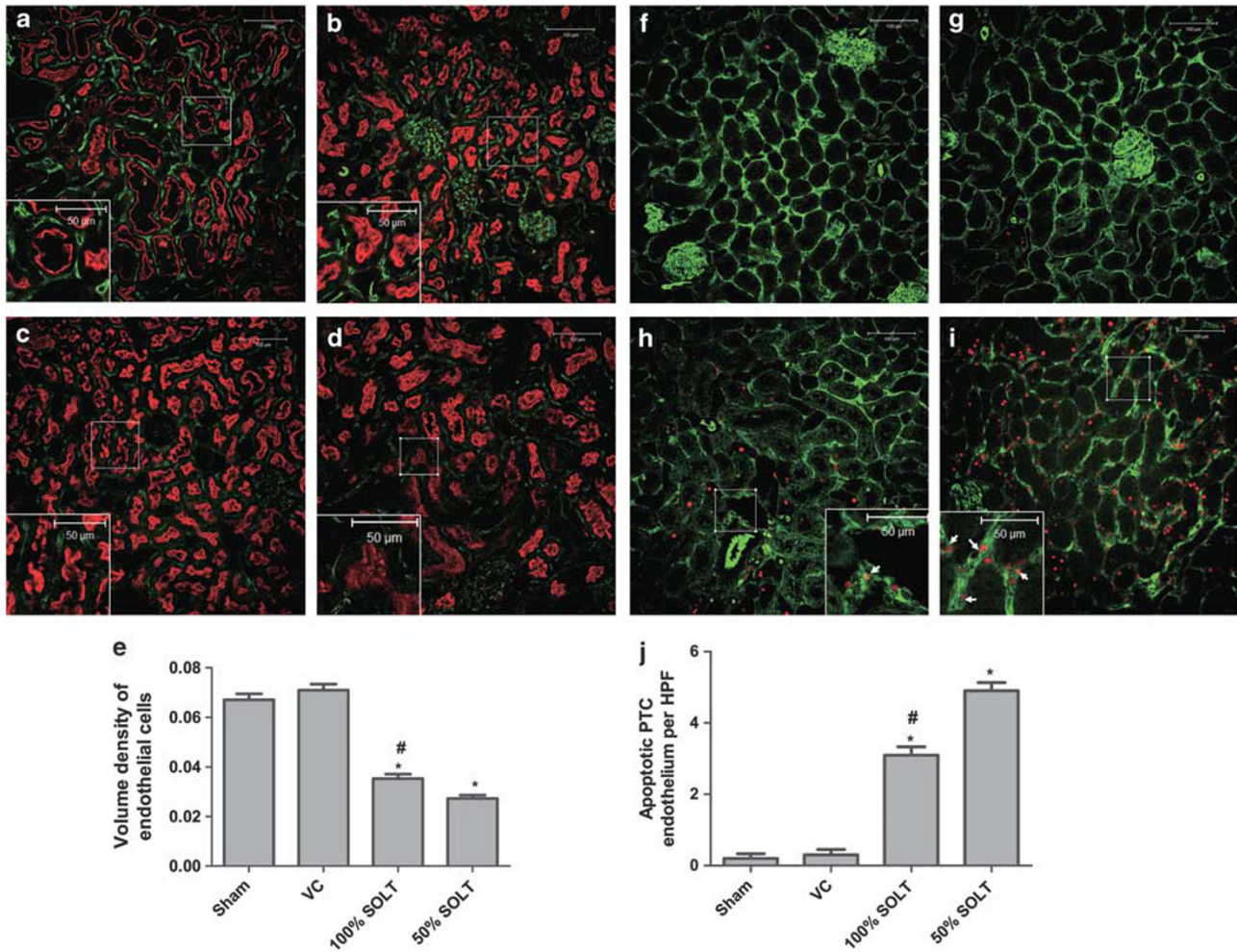
Figure 7 Detection of PTC endothelial injury in the kidney postoperatively. (**a–d**) Representative fluorescence photomicrographs obtained at 24 h postoperatively to detect PTC integrity. Co-staining with RECA (green) and rhodanmine-labeled LCA (red) identified PTC endothelial cells. Selected areas were digitally enlarged to show PTC morphology. (**a**) Sham-operated group; (**b**) vessel-clamped group; (**c**) 100% SOLT group; (**d**) 50% SOLT group. (**e**) Quantification of PTC endothelial cells was performed on 10 images/slide and expressed as endothelium volume density per high power field ($n = 6$). Data are expressed as the mean ± s.e.m. *$P < 0.05$ *versus* sham and VC; #$P < 0.05$ *versus* 50% SOLT. (**f–h**) Representative fluorescence photomicrographs obtained at 6 h postoperatively to detect apoptosis in the PTC endothelium. Co-staining with RECA (green) and TUNEL (red) identified PTC endothelial apoptosis. (**f**) Sham-operated group; (**g**) vessel-clamped group; (**h**) 100% SOLT group; (**i**) 50% SOLT group. (**j**) The number of TUNEL-positive PTC endothelial cells was quantified on 10 images/slide and expressed as cells per high power field ($n = 6$). Data are expressed as the mean ± s.e.m. *$P < 0.05$ *versus* sham and VC; #$P < 0.05$ *versus* 50% SOLT. Scale bars: 100 μm.
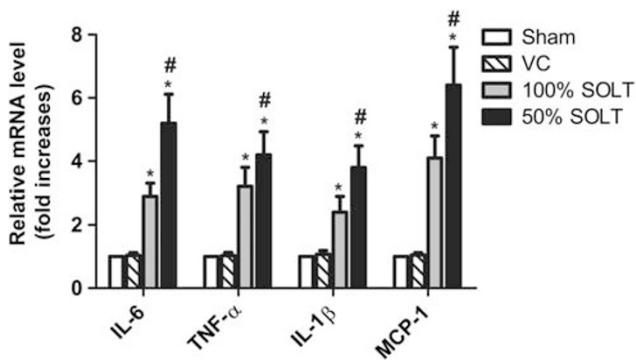

Figure 8 Detection of inflammatory cytokines in liver tissue. The mRNA level was detected at 6 h postoperatively. Quantifications of TNF-α, IL-1β, IL-6, and MCP-1 mRNAs are normalized to GAPDH ($n = 6$). Data are expressed as the mean ± s.e.m. *$P < 0.05$ *versus* sham and VC; #$P < 0.05$ *versus* 50% SOLT.

Maintenance of PTC integrity depends on the angio-regulatory proteins present in renal tissue. In our study, we found decreased VEGF and increased TSP-1 and MMP9 expression in renal tissue post-LT. VEGF is constitutively expressed in podocytes and tubular cells with trophic, survival, and angiogenic properties.[15] In the renal IRI and nephrotoxic AKI model, Basile *et al*[16] and Yuan *et al*[17] reported VEGF downregulation in renal tubular cells. Leonard *et al*[18] demonstrated that VEGF-121 attenuated IRI-induced loss of renal microvasculature. VEGF inhibited by the VEGF receptor-1 decreases VEGF activity and induces endothelial cell apoptosis.[19] The reduction of VEGF expression in SOLT rat kidneys is an important explanation for PTC rarefaction. As an antiangiogenic factor, TSP-1 can inhibit endothelial cell proliferation and induce endothelial cell apoptosis. In the IRI
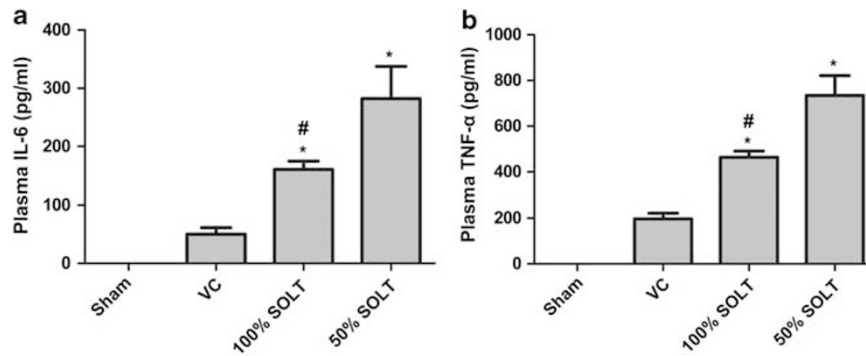
Figure 9 Detection of plasma TNF-α and IL-6 levels. (a) Plasma IL-6 expression; (b) plasma TNF-α expression. Serum was collected at 6 h postoperatively (n = 6). Data are expressed as the mean ± s.e.m. *P < 0.05 versus sham and VC; #P < 0.05 versus 50% SOLT.

model, TSP-1 expression increases as early as 3 h post reperfusion and TSP-1 upregulation results in an increased expression of caspase-3 in the renal tubule.[20] The renal expression of TSP-1 correlates with the loss of PTC integrity in a remnant kidney model.[21] Another antiangiogenic factor, MMP-9, is a proteinase which inhibits angiogenesis by mediating the generation of angiostatin. Angiostatin inhibits angiogenesis and promotes endothelial apoptosis.[22] Increased MMP-9 activity has been found in the renal IRI model and is related to endothelial injury.[23]

In our study, the inflammatory response was considered an important priming factor for post-LT renal injury. We found IL-1β, IL-6, TNF-α, and MCP-1 upregulation in liver tissue 6 h post-LT. The serum concentration of IL-6 and TNF-α was also increased at 6 h post-LT. The activated inflammatory response in renal tissue consisted of increased macrophage infiltration and upregulated IL-1β, IL-6, and TNF-α. The graft IRI induced the infiltration of leukocytes and liver cell injury. Proinflammatory cytokines were released from leukocytes and injured liver cells. These cytokines likely aggravate graft injury and promote the systemic inflammatory response.[24] The systemic inflammatory response, including upregulated expression of serum IL-6 and TNF-α, has been found in a rat model of liver IRI.[25] The circulating pro-inflammatory cytokines can act on distant organs such as the lung and kidney.[26,27] IL-6 and TNF-α can promote an inflammatory reaction in the kidney by upregulating endothelial adhesion molecules such as selectin and intercellular adhesion molecule-1. The upregulated adhesion molecules induce leukocyte recruitment and extravasation into the interstitial space.[28] These leukocytes, including macrophages, activate an inflammatory cascade causing upregulation of pro-inflammatory cytokines and tissue injury.[29] Macrophages contribute to the initiation of tissue damage in models such as kidney allograft rejection and lung IRI.[30,31] Early macrophage depletion could obviously attenuate renal tubule injury in the rat renal IRI model.[32] Increased macrophage infiltration also enhances PTC endothelial injury. Qi et al[33] reported that macrophage depletion prevents microvasculature loss in murine models of kidney transplantation.

In our study, we found no obvious renal injury in VC rats, and more marked injury in 50% SOLT rats compared with 100% SOLT rats. The VC group was designed to simulate renal hemodynamic instability caused by IHIVC clamping during surgery. Our findings suggest that intraoperative hemodynamic compromise to the kidneys does not play a major role in post-LT AKI. This conclusion is in contrast to that of Park et al,[34] who found increased renal IRI injury with renal vein clamping compared with arterial clamping in a Fisher rat model. In response, we suggest that the difference between rat strains should also be considered. The 50% SOLT group was designed to assess the effect of graft function on post-LT AKI. In the reduced size liver graft, the inflammatory response and sinusoidal endothelial injury are more severe,[35] inducing more significant hepatocyte injury and liver dysfunction. More inflammatory cytokines are released, affecting end-organ function. This would explain the observed post-LT AKI in the 50% SOLT group. This finding confirms that in the literature, demonstrating a high prevalence of AKI in patients receiving reduced size versus full-size grafts.[36]

This is the first study of post-LT AKI in a SOLT animal model. The relationship between liver IRI and renal dysfunction has been recently reported. Lee et al[12] studied AKI in a liver IRI model and designed a model to study AKI associated with acute liver failure. Compared with the liver IRI animal model, the SOLT model is more applicable to human LT. The anhepatic stage and graft cold ischemia reperfusion can only be simulated in a SOLT animal model. Thus, we conclude that our research further contributes to understanding liver graft dysfunction and distant organ injury.

Our study has several limitations. We focused on the short-term effects of liver graft function on post-LT AKI; some important risk factors of AKI in human LT are not included in our study. By using syngeneic rats we did not require immunosuppressive anti-rejection therapy. In human LT, the systemic inflammatory response caused by rejection and the nephrotoxic effects caused by immunosuppression therapy are important risk factors for post-LT AKI.[6] Another
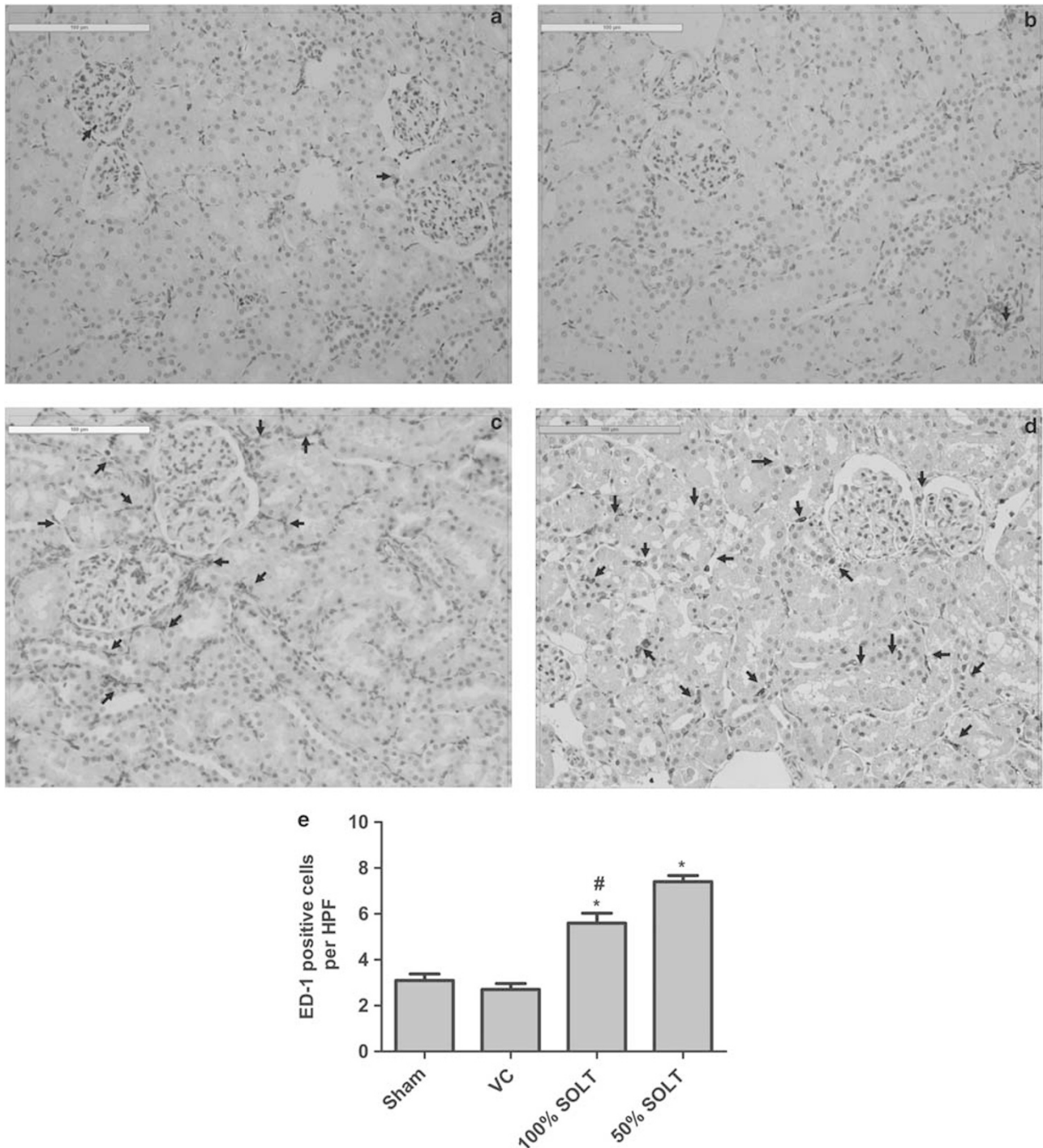
Figure 10 Detection of macrophage infiltration in the kidney. Representative immunohistochemical photomicrographs obtained at 24 h after reperfusion. (**a**) Sham-operated group. (**b**) Vessel-clamped group. (**c**) SOLT group (100%). (**d**) SOLT group (50%). (**e**) Quantification of infiltrated macrophages was performed for 10 images/slide and expressed as ED-1-positive cells per high power field ($n = 8$). Data are expressed as the mean ± s.e.m. *$P < 0.05$ *versus* sham and VC; #$P < 0.05$ *versus* 50% SOLT. Scale bars: 100 μm.

limitation was that the operation was carried out between healthy animals. Some patients with chronic liver failure have hepatorenal syndrome, making pre-LT renal insufficiency an important risk factor for post-LT AKI.[6] We did not simulate chronic liver disease in our rat recipients and could therefore not study the effect of pre-LT renal insufficiency on post-LT AKI. We also noticed that the long-term effects of LT on the kidneys needed to be clarified in the future study.
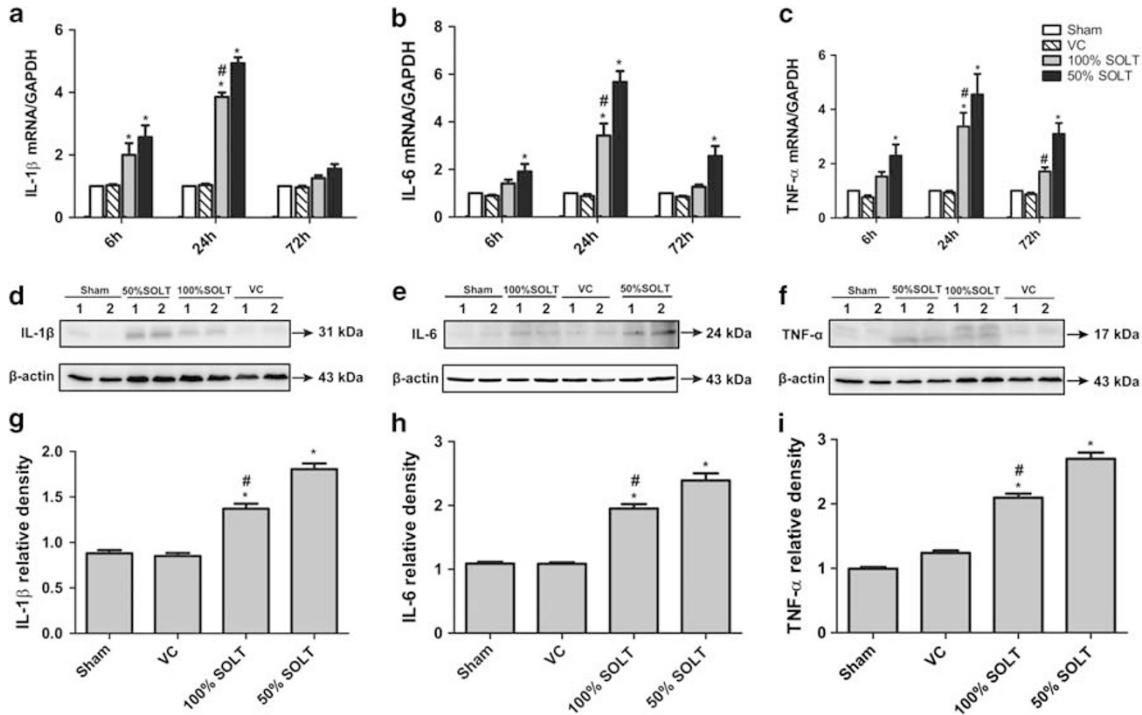
Figure 11 Detection of inflammatory cytokines in the renal tissue. The mRNA level was detected at 6, 24, and 72 h postoperatively, and protein level was detected at 24 h postoperatively. (a–c) Quantifications of TNF-α, IL-1β, and IL-6 mRNAs were normalized to GAPDH ($n = 6$ for 6 h, 8 for 24 h, 6 for 72 h). (d–f) Representative immunoblot of TNF-α, IL-1β, and IL-6 protein expression in kidney tissue homogenates. (g–i) Densitometric quantifications of TNF-α, IL-1β, and IL-6 normalized to actin ($n = 8$). Data are expressed as the mean ± s.e.m. *$P < 0.05$ versus sham and VC; #$P < 0.05$ versus 50% SOLT.
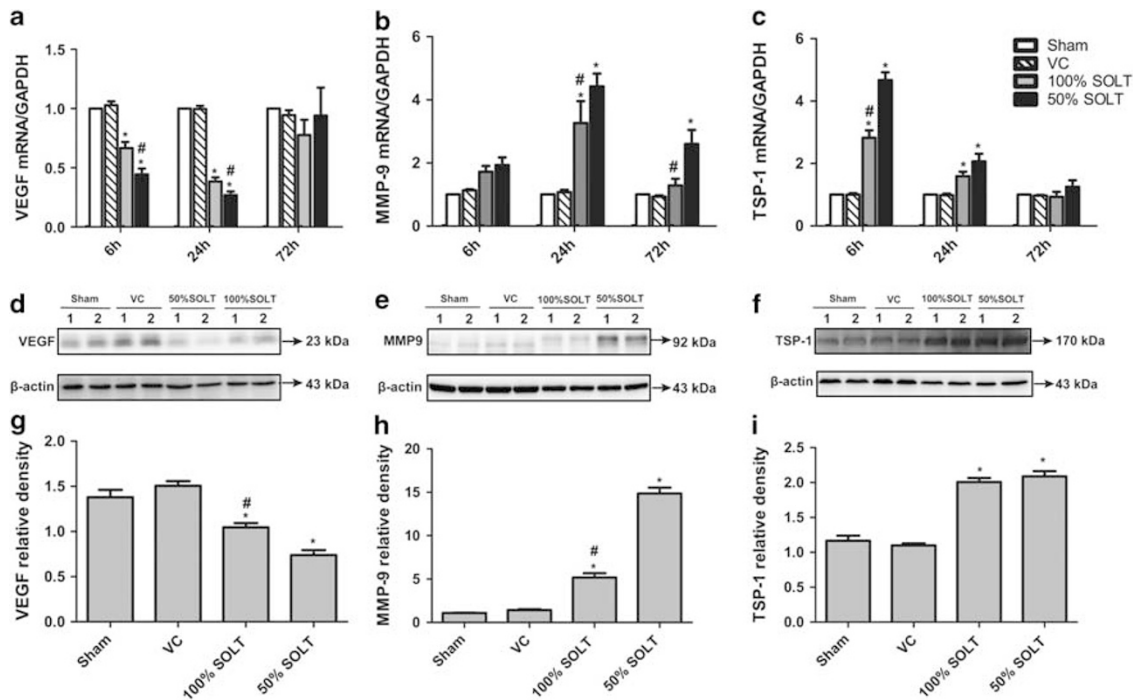

Figure 12 Detection of VEGF, MMP9, and TSP-1 in renal tissue. The mRNA level was detected at 6, 24, and 72 h postoperatively and the protein level was detected 24 h postoperatively. (a–c) Quantifications of VEGF, MMP9, and TSP-1 mRNAs were normalized to GAPDH ($n = 6$ for 6 h, 8 for 24 h, 6 for 72 h). (d–f) Representative immnuoblotting of VEGF, MMP9, and TSP-1 protein expressions in kidney tissue homogenates. (g–i) Densitometric quantifications of VEGF, MMP9, and TSP-1 normalized to actin ($n = 8$). Data are expressed as the mean ± s.e.m.*$P < 0.05$ versus sham and VC; #$P < 0.05$ versus 50% SOLT.

In conclusion, we have elucidated the effects of AKI post-LT in a rat SOLT model. Effective interventions to protect graft function and inhibit the systemic inflammatory response, in order to reduce post-LT AKI require further research.

DISCLOSURE/CONFLICT OF INTEREST
The author declares no conflict of interest.

1. Biancofiore G, Davis CL. Renal dysfunction in the perioperative liver transplant period. Curr Opin Organ Transplant 2008;13:291–297.
2. Chertow GM, Burdick E, Honour M, *et al*. Acute kidney injury, mortality, length of stay, and costs in hospitalized patients. J Am Soc Nephrol 2005;16:3365–3370.
3. Fisher NC, Nightingale PG, Gunson BK, *et al*. Chronic renal failure following liver transplantation: a retrospective analysis. Transplantation 1998;66:59–66.
4. Cohen AJ, Stegall MD, Rosen CB, *et al*. Chronic renal dysfunction late after liver transplantation. Liver Transplant 2002;8:916–921.
5. Gonwa TA, Mai ML, Melton LB, *et al*. End-stage renal disease (ESRD) after orthotopic liver transplantation (OLTX) using calcineurin-based immunotherapy: risk of development and treatment. Transplantation 2001;72:1934–1939.
6. Pham PT, Pham PC, Wilkinson AH. Management of renal dysfunction in the liver transplant recipient. Curr Opin Organ Transplant 2009;14:231–239.
7. Kamada N, Calne RY. Orthotopic liver transplantation in the rat. Technique using cuff for portal vein anastomosis and biliary drainage. Transplantation 1979;28:47–50.
8. Omura T, Ascher NL, Emond JC. Fifty-percent partial liver transplantation in the rat. Transplantation 1996;62:292–293.
9. Morigi M, Introna M, Imberti B, *et al*. Human bone marrow mesenchymal stem cells accelerate recovery of acute renal injury and prolong survival in mice. Stem Cells 2008;26:2075–2082.
10. Kwon O, Hong SM, Sutton TA, *et al*. Preservation of peritubular capillary endothelial integrity and increasing pericytes may be critical to recovery from postischemic acute kidney injury. Am J Physiol Renal Physiol 2008;295:F351–F359.
11. Basile DP, Donohoe D, Roethe K, *et al*. Renal ischemic injury results in permanent damage to peritubular capillaries and influences long-term function. Am J Physiol Renal Physiol 2001;281:F887–F899.
12. Lee HT, Park SW, Kim M, *et al*. Acute kidney injury after hepatic ischemia and reperfusion injury in mice. Lab Invest 2008;89:196–208.
13. Bombeli T, Karsan A, Tait JF, *et al*. Apoptotic vascular endothelial cells become procoagulant. Blood 1997;89:2429–2442.
14. Nangaku M. Chronic hypoxia and tubulointerstitial injury: a final common pathway to end-stage renal failure. J Am Soc Nephrol 2006;17:17–25.
15. Schrijvers BF, Flyvbjerg A, De Vriese AS. The role of vascular endothelial growth factor (VEGF) in renal pathophysiology. Kidney Int 2004; 65:2003–2017.
16. Basile DP, Fredrich K, Chelladurai B, *et al*. Renal ischemia reperfusion inhibits VEGF expression and induces ADAMTS-1, a novel VEGF inhibitor. Am J Physiol Renal Physiol 2008;294:F928–F936.
17. Yuan H, Li X, Pitera JE, *et al*. Peritubular capillary loss after mouse acute nephrotoxicity correlates with down-regulation of vascular endothelial growth factor-A and hypoxia-inducible factor-1{alpha}. Am J Pathol 2003;163:2289–2301.
18. Leonard EC, Friedrich JL, Basile DP. VEGF-121 preserves renal microvessel structure and ameliorates secondary renal disease following acute kidney injury. Am J Physiol Renal Physiol 2008;295: F1648–F1657.
19. Marco GSD, Reuter S, Hillebrand U, *et al*. The soluble VEGF receptor sFlt1 contributes to endothelial dysfunction in CKD. J Am Soc Nephrol 2009;20:2235–2245.
20. Thakar CV, Zahedi K, Revelo MP, *et al*. Identification of thrombospondin 1 (TSP-1) as a novel mediator of cell injury in kidney ischemia. J Clin Invest 2005;115:3451–3459.
21. Kang D, Joly AH, Oh S, *et al*. Impaired angiogenesis in the remnant kidney model: I. potential role of vascular endothelial growth factor and thrombospondin-1. J Am Soc Nephrol 2001;12:1434–1447.
22. Basile DP, Fredrich K, Weihrauch D, *et al*. Angiostatin and matrix metalloprotease expression following ischemic acute renal failure. Am J Physiol Renal Physiol 2004;286:F893–F902.
23. Caron A, Desrosiers RR, Beliveau R. Ischemia injury alters endothelial cell properties of kidney cortex: stimulation of MMP-9. Exp Cell Res 2005;310:105–116.
24. Lemasters JJ, Thurman RG. Reperfusion injury after liver preservation for transplantation. Annu Rev Pharmacol Toxicol 1997;37:327–338.
25. Wanner GA, Ertel W, Muller P, *et al*. Liver ischemia and reperfusion induces a systemic inflammatory response through Kupffer cell activation. Shock 1996;5:34–40.
26. Park SW, Chen SW, Kim M, *et al*. Human activated protein C attenuates both hepatic and renal injury caused by hepatic ischemia and reperfusion injury in mice. Kidney Int 2009;76:739–750.
27. Franco-Gou R, Rosello-Catafau J, Peralta C. Protection against lung damage in reduced-size liver transplantation. Crit Care Med 2006;34:1506–1513.
28. Molitoris BA, Sandoval R, Sutton TA. Endothelial injury and dysfunction in ischemic acute renal failure. Crit Care Med 2002;30:S235–S240.
29. Bonventre JV, Weinberg JM. Recent advances in the pathophysiology of ischemic acute renal failure. J Am Soc Nephrol 2003;14:2199–2210.
30. Jose MD, Ikezumi Y, van Rooijen N, *et al*. Macrophages act as effectors of tissue damage in acute renal allograft rejection. Transplantation 2003;76:1015–1022.
31. Zhao M, Fernandez LG, Doctor A, *et al*. Alveolar macrophage activation is a key initiation signal for acute lung ischemia-reperfusion injury. Am J Physiol Lung Cell Mol Physiol 2006;291:L1018–L1026.
32. Jo S, Sung S, Cho W, *et al*. Macrophages contribute to the initiation of ischaemic acute renal failure in rats. Nephrol Dial Transplant 2006;21:1231–1239.
33. Qi F, Adair A, Ferenbach D, *et al*. Depletion of cells of monocyte lineage prevents loss of renal microvasculature in murine kidney transplantation. Transplantation 2008;86:1267–1274.
34. Park Y, Hirose R, Dang K, *et al*. Increased severity of renal ischemia-reperfusion injury with venous clamping compared to arterial clamping in a rat model. Surgery 2008;143:243–251.
35. Man K, Lo C, Ng IO, *et al*. Liver transplantation in rats using small-for-size grafts: a study of hemodynamic and morphological changes. Arch Surg 2001;136:280–285.
36. Gajate L, Martin A, Elias E, *et al*. Analysis of renal function in the immediate postoperative period after partial liver transplantation. Liver Transplant 2006;12:1371–1380.